

# **ANALYSIS OF ROCK MICROSTRUCTURE USING HIGH-RESOLUTION X-RAY TOMOGRAPHY**

A.P. Sheppard, R. M. Sok, H. Averdunk, V. B. Robins and A. Ghous  
Mesoscale Physics Group, Applied Mathematics, ANU

*This paper was prepared for presentation at the International Symposium of the Society of Core Analysts held in Trondheim, Norway 12-16 September, 2006*

## **ABSTRACT**

In previous work we have described and validated robust techniques for partitioning the pore space of a porous material into simple regions, thereby allowing it to be represented by a network of simple building blocks. The primary purpose of this analysis is the generation of a pore-throat network for modelling immiscible multi-phase fluid displacements. However, combining our partitioning algorithms with recently developed methods for studying complex and disordered networks, and geometric studies of the building blocks themselves, results in powerful tools for characterising rock microstructure.

We extend this approach by applying the analysis to both the pore space and its complement, the grain space. Partitioning the grain space has particular meaning for clastic rocks where it is equivalent to identifying individual grains. Studying the two interpenetrating networks that result gives us a more complete description of the material, and in particular, gives us the chance to study causal relationships linking microstructure to macroscopic properties.

We apply this methodology to a selection of clastic and carbonate rock images from the library of samples imaged at the ANU X-Ray micro-CT facility. For the clastic samples, we are able to assess whether differences in porosity and connectivity are the result of variations in grain size, grain shape or packing efficiency. For all samples, we look at the robustness and usefulness of several characterisation measures.

## **INTRODUCTION**

X-ray microcomputed tomography (XCT), with its capacity to provide extremely detailed three-dimensional images at the pore-scale, is increasingly seen as an important complement to experiment in the analysis of rock core. The power of tomographic analysis rests on two main capabilities. Firstly, with the capacity to give results more quickly than special core analysis, and to study drill fragments (Arns et al 2005), it allows the sampling of a much wider range of core material. Secondly, it may help provide answers to questions of causality: Why is this core more permeable? Why is the residual oil higher in that core? Why does this one exhibit stronger imbibition rate effects at low capillary numbers? Understanding some of the underlying causes of variations in rock properties has great potential to assist in the assessment of anomalous experimental results, and ultimately to reduce uncertainty in prediction.

This paper will concern itself with the second capability, which remains, to a large degree, unrealised. It must first be recognised that answers to the "Why?" questions of

core analysis are often based in chemistry rather than microstructure. XCT may, in the future, help to characterise reservoir wettability and allow the direct observation of dynamic displacements, thus helping to resolve questions of chemistry. However, such research is well beyond the scope of this work, where we limit ourselves to an investigation of causes and consequences of microstructural variation.

A key tool in the quantitative assessment of structure is partitioning. Breaking a complex object down into simple building blocks enables one to analyse the geometrical characteristics of each component, while also studying the topological and statistical properties of the structure as a whole. In a porous material, one can apply a partitioning analysis to either the grain space or the pore space; in this work we will do both.

Early quantitative studies of grain structure looked predominantly at the packing of equal spheres, and were hamstrung by a shortage of experimental data. Finney (1970), Blunt and Bryant (1992), Bryant et al (1996) all used the same data set, the Finney pack, containing around 8000 equal ball bearings. XCT is now solving this shortcoming, as evidenced by Aste (2006), who used multiple XCT data sets, each with up to 150,000 beads to find "universal" scaling behaviour of Delaunay cell volumes. Indeed, Delaunay analysis, which partitions space into tetrahedral cells whose vertices correspond to sphere centers, has been the basic analytic tool in such studies. Delaunay analysis is most relevant for packings of identical spheres, although some authors have also considered nonidentical spheres (Richard et al 2001) and non-spherical grains (Luchnikov et al 1999), with limited success.

Studies of pore structure are normally driven by the desire to model single and multi-phase flow properties. A number of algorithms for partitioning have been proposed, based on either the medial axis transform (Lindquist et al 1996, Liang et al 2000, Al Raoush et al 2005, Sheppard et al 2005) or maximal balls of the covering radius map (Silin and Patzek 2003), usually with the primary aim of generating input for pore scale network modelling codes that simulate drainage and imbibition. Other works have exploited complementarity of the pore and grain spaces. Bryant and Mellor (1996) use the fact that the centers of Delaunay tetrahedra in a sphere pack are located at pore body centers, and that their faces correspond to pore throats, to build a network representation of the pore space of the Finney pack. Bakke and Oren (1997) use a similar approach – the dilation of predetermined grains to form a quasi-Voronoi tessellation – to construct networks from process-based models of granular materials.

Thompson et al (2006) is the nearest ancestor of the current work, describing an algorithm for building pore-networks from partitions of the grain phase. The grain partition is performed using a watershed transformation (as does the algorithm we present here); pore centers are then identified from a morphological analysis of the pore space in each Delaunay tetrahedron. Pore partitioning is done via the watershed transform, and some pore merging is subsequently performed to eliminate over-partitioning. The authors carefully checked the efficacy of their method on synthetic sphere packs, but need to do much more for non-spherical grains, as they only studied a single sandstone sample imaged with rather low quality. The network from this single sample exhibits some odd properties: low coordination numbers, little difference between pore and throat radii and an abundance of small pores at or near the voxel resolution.

While these features may be a consequence of inadequate image quality, their extremely promising method certainly remains unproven.

## PROCEDURES

This study looks at 8 samples: 2 unconsolidated cores (labeled U1 and U2), 3 sandstones (S1, S2, S3), 2 carbonates (C1 and C2) and a packing of mono-dispersed acrylic spheres (P1). U1 is an unconsolidated sand pack from South East Australia; U2 is a poorly consolidated reservoir sandstone. S1 and S2 are different pieces taken from the same 40mm core plug of Castlegate sandstone. S3 is a Berea sandstone, while C1 is a Mt Gambier limestone and C2 a vuggy carbonate from west Texas. S1 and S2 are particularly interesting since they were acquired at slightly different resolutions, while segmentation was performed independently, without any cross-checking, by two different operators, yielding porosity values of 26% and 21%. These samples represent a good test since we do not know whether the difference in porosity is a result of differences in acquisition and segmentation, or a genuine difference in microstructure.

Images of all samples were captured on the ANU XCT facility (Sakellariou et al 2003). These images, comprising up to  $2000^3$  voxels each, were filtered with anisotropic diffusion and segmented using the technique of converging active contours, all as outlined elsewhere (Sheppard et al 2003). A subset wholly contained within each cylindrical core was taken from each image, for convenience. Details of the samples and the subsets used can be found in Table 1, and slices through the reconstructed images are shown in Figure 1.

The pore and the grain space were each analysed separately using a multi-stage approach. For the pore space analysis, we first removed disconnected components from both the pore and grain phase, then calculated the Euclidean distance map, followed by the covering radius map (Hilpert and Miller 2001, Silin et al 2003) to pin potential pore centers, and then the distance-centered medial axis transform (Pudney 1998) of each phase. This enabled the pore body region centers to be identified, thus forming a network of junctions and links. A watershed transform was then applied to the remaining region centers to fully identify each region, thereby partitioning the full pore space. This network was simplified using a carefully designed region-merging algorithm (Sheppard et al 2005). Finally, throats were assigned a portion of the volume in each pore.

The grain space was analysed using a very similar approach to the pores, and a similar method to that used by Thompson et al (2006). Euclidean distance and covering radius maps were calculated. Next, grain centers were identified as those voxels that were not covered by a larger radius in the covering radius map – “master” voxels in the parlance of Silin and Patzek (2003). These centers were used to seed a watershed transform based on the Euclidean distance map, which partitions the grain space into regions whose boundaries coincide with constrictions of the grain space. To overcome the over-partitioning that seems inevitable with these methods, the aforementioned region-merging algorithm was applied to this partitioning to remove spurious grains.

Analysed in isolation, these partitions provide a wealth of information about the microstructure, since we can characterise the topology of the connection networks and the geometry of the individual pores and grains in as much detail as is desired. Here we

restrict ourselves to measuring geometry through radius (maximum inscribed sphere radius for pores and grains; maximum inscribed sphere radius at the minimum constriction for throats and grain contacts), aspect ratio (ratio between pore/grain radius and the radius of each neighbouring throat/grain contact) and sphericity (ratio between the pore, grain or throat radius and the radius of a sphere with the same volume as the pore, grain or throat), while we characterise topology through genus (measured per unit volume) coordination numbers and ring sizes (rings are minimal closed paths on the network, where a minimal closed path is one having no shortcuts across it).

All algorithms used on voxelated data are written in C++ and fully parallelised using the Message Passing Interface (MPI). Analysis is carried out on 1.4GHz Itanium processors in the SGI Altix 3700 at the Australian Partnership for Advanced Computation's National Facility. The full analysis, typically on 64 processors, takes between 30 minutes and 3 hours, using around 12 bytes/voxel, with processing times strongly dependent on the sample morphology. Extrapolation of run times indicates that analysis of images much larger than this will be feasible with no changes to either hardware or software.

## RESULTS

First, to validate our approach, we analyse a typical random sphere pack, with packing density of 62% and composed of approximately 8000 acrylic spheres 1.6 mm in diameter. This was imaged in the ANU XCT facility at a resolution of 17 microns. With a large sphere diameter – 90 voxels, and excellent contrast and signal to noise ratio in the image, the segmentation of this data set and identification of individual spheres is very easy. We study a 512x512x512 voxel subset, which we believe to be of sufficient size to be representative. Boundary effects are minimized by ignoring data that involves spheres which touch the boundary. Figure 2 shows raw image data and the results of grain and pore identification. The mean radius of the identified grains (away from the image boundary) is 0.793mm, with all radii between 0.791 and 0.797mm, indicating excellent sphere identification. The mean sphere coordination number is 6.2, with a standard deviation of 1.4. We imagine this to be a slight over-estimate due to some near-neighbours being mis-identified as touching. The pore space analysis shows an average pore coordination number of 6.5.

To investigate the duality relationship between the pore and grain space partitions, we performed a Delaunay triangulation using the grain centers. This tessellates space into tetrahedra whose vertices are at the grain centers. The main question is whether much can be inferred about the structure of the pore network from an analysis of the grain contact network, i.e. whether there is much correspondence between the pore bodies and the Delaunay tetrahedra. To do this, we simply counted the number of pore centers in each Delaunay tetrahedron. In a perfectly dual structure, there would be a single pore in every tetrahedron, at its center. The triangulation yields 310 tetrahedra away from the image boundary. Only 86 (28%) of these tetrahedra contain a pore center, which is inevitable since there are only 86 pores in this volume. We were initially concerned that this result may be a consequence of too much pore merging. However, very little changes when the pore merging is turned off altogether: most pores are still surrounded by much more than 4 spheres. This result shouldn't be surprising since even in a close packing of spheres, one-third of the cavities are octahedral. In addition, the work of Al-

Raoush et al (2005) showed that equivalent pore networks are more than 4-connected in random sphere packings. Figure 3(a) shows the configuration of a typical pore that spans 3 tetrahedra, which confirms that there is indeed no constriction corresponding to most Delaunay faces. The geometry of the tetrahedra can be used to help explain this: 35% of them don't contain their own circumcenter, indicating highly asymmetric shapes, while figure 3(b) shows that the Delaunay edge lengths are distributed over a wide range, inferring that the vast majority of tetrahedra are far from regular.

Next, we examine the effectiveness of our grain partitioning algorithm for sample U1. This type of unconsolidated material should not be very difficult to partition - certainly the human eye can identify grains with great confidence. The partitioning of a slice of U1 can be seen in figure 5. While it is clear that the great majority of grains have been well identified, some anomalies are apparent. Firstly, some grains appear to be divided unnecessarily. We believe that this does not usually signify a problem with the algorithm; rather, the human eye makes incorrect assumptions about 3D structure from incomplete information in the 2D section. Secondly, some disk- and rod-like grains have not been correctly partitioned (see inset in figure 5). This is a result of the fact that genuine constrictions are not picked up by the maximal ball approach if they are shorter than they are wide – see figure 5 for more details – since the maximal Euclidean spheres “bottom out” on the far side of the grain, rather than being limited by the constriction. This highlights a fundamental drawback in all morphological analysis that is based on spheres – it does not deal well with anisotropic structures. If your material is made up of spheroids, then far better to probe its structure with a “spheroid distance transform” rather than use the Euclidean distance map. Currently this isn't an option; one must use the Euclidean distance map, but remain aware of its limitations.

Returning to sample U1: apart from these relatively minor issues, visual inspection of the section in figure 5, combined with a very high mean aspect ratio of 4.5 (see Table 3) indicate that the partition is good enough to yield high quality data.

An important question to ask when working with XCT data is to what degree the results are limited by the voxel resolution. This can be answered in part by checking the throat size distribution. If the identified throat channels are predominantly distributed well above the voxel resolution, then it is reasonable to assume, in the absence of other evidence to the contrary, that an increase in resolution (decrease in voxel size) would not add a significant number of new throats. U1 and U2 both exhibit throat distributions that seem to taper out before the resolution limit. S3 and the carbonates, on the other hand, all have throat radius distributions that peak at or near the voxel size. This implies a great many very narrow throats, leading one to assume that the XCT image has failed to capture enough feature. Very small-scale feature usually has little impact on permeability but can strongly affect porosity and residual saturations. Integrating sub-voxel features with XCT image data is an ongoing research project within our research group.

Let us consider again samples S1 and S2, taken several centimetres apart from the same core of Castlegate sandstone, and the question of whether these samples are physically different, or just appear that way after undergoing different image acquisition and segmentation. The grain partitions are strikingly similar – S1 has marginally smaller

grains and a slightly lower grain coordination, but the similarity of the distributions as shown for grain equivalent sphere radii in figure 4(a) leads one to conclude that the two samples are composed of the same grains. Now, a 2% variation in the grain radii corresponds to a 6% change in the grain volumes, which would be expected to lead to exactly the observed 5% difference in porosity if the grain packing density is unchanged. Indeed, our results show both samples to have 179 grains/mm<sup>3</sup>, strongly suggesting that the rock samples S1 and S2 are statistically equivalent. These relatively minor differences in grain size result in far more marked variations in pore space properties, as can be seen in Table 3 and for the pore equivalent sphere radius in figure 4(b). This result supports the contention of Thompson et al (2005) that grain partition algorithms are more robust than pore space analyses.

Tables 2 and 3 show topological and geometric attributes of the partitions of the pore and grain space respectively. It is clear from the slice and network images that the carbonates have an extremely different structure to the clastic. However, the unweighted average properties do not exhibit this fact clearly. This is because the very large structures that dominate the carbonates are numerically insignificant. If, on the other hand, these distributions are weighted by the volume of the contributing element, then the carbonates emerge as being starkly different, with average coordination numbers and aspect ratios above 20. Another advantage of weighting by volume is that small features, which are more sensitive to noise, play a smaller role, reducing the overall noise sensitivity of the results.

## DISCUSSION

The analysis of samples S1 and S2, taken from the same plug, is both unsettling and encouraging. It is very encouraging because we have demonstrated the ability of the grain partitioning method to determine statistical equivalence between different data sets. On the other hand, almost any calculation performed on the segmented pore spaces would return significantly different results for S1 than for S2. Reducing the uncertainties associated with segmentation therefore remains a very high priority.

Network extraction algorithms consists essentially of 3 steps: firstly, to identify potential pore centers, secondly to partition the pore space using the pore centers as seeds, and thirdly to merge pores that appear to be part of the same body. Although the second and third tasks are critically important, there is little disagreement on the best methods to use. The major current question for network generation algorithms is therefore deciding how to perform stage 1. Three methods have been proposed for locating pore centers: as junctions of the medial axis, as centers of maximal balls from the covering radius transform, or as centers of Delaunay tetrahedral resulting from a prior partitioning of the grain space.

Basing a partitioning method on the medial axis has the fundamental advantage that the final partitioning will be faithful to the topology of the original object. It is therefore robust to small changes in the object that don't alter the topology. It has the disadvantage that medial axis junctions do not necessarily correspond to maxima of the Euclidean distance map – in fact, in a complex pore space, they correspond only rarely.

Based on our experience, and based on a number of networks published in the literature

(Silin and Patzek 2003, Al Raoush et al 2005, Thompson et al 2005), the covering sphere algorithm alone is too noise sensitive, so that the connectivity of the generated network bears little relation to the original object. To be specific, the generated network will be full of rings - in which residual fluids may be trapped - that do not correspond to any feature in the object.

The new method of Thompson, using Delaunay tetrahedra, has similar advantages and disadvantages to the medial axis approach, while being limited to granular packs. It is extremely robust, but it is also unclear in a non-spherical packing whether there is a strong correspondence between Delaunay tetrahedra and the morphology of the pore space. As we have shown, there is a serious breakdown in this correspondence even for packings of identical spheres.

## CONCLUSIONS

This work lays the foundation for a future study, both more extensive and intensive than the present one, on causal relationships in granular materials. The main results of this preliminary work are:

- Grain partitioning, performed by a watershed transform that is seeded by centers of maximal covering spheres and followed by grain merging, can be successful for identifying grains in clastic rocks.
- The grain partitioning is very robust to variations in acquisition and segmentation parameters. This appears to result from the fact that methods based on the Euclidean distance map work best for identifying large grains with relatively convex and isotropic shapes.
- The pore-space analysis is much less robust, due to the less predictable shapes of pore bodies and because of the important role played by throats that are often only 2-3 voxels in diameter, and therefore very sensitive to small parameter variations.
- When characterising a material by network parameters such as aspect ratio, it is valuable to weight the distributions by pore or grain volume. If this is not done, one can miss the effect of heterogeneity exhibited by carbonates.
- Even in a packing of identical spheres, the correspondence between pore centers and the tetrahedra formed from a Delaunay triangulation of grain centers is not well defined. More investigation is required to quantify the correspondence between Delaunay tetrahedra and pore bodies in more realistic packings.

## NOMENCLATURE

$r_g, r_p, r_t$	grain, pore, throat radius ( $\mu\text{m}$ )	$G$	genus (topo) density ( $\text{mm}^{-3}$ )
$N_g, N_p, N_t$	Total # of grains, pores, throats	$S_g, S_p$	grain, pore sphericity
$Z_g, Z_p$	grain, pore coordination number	$\langle \rangle_N$	unweighted average
$D_g, D_p$	grain, pore density ( $\text{mm}^{-3}$ )	$\langle \rangle_V$	volume weighted average
$AR_g, AR_p$	aspect ratio of grains/contacts, pores/throats		
$esr_g, esr_p$	grain, pore equivalent sphere radius ( $\mu\text{m}$ )		

## REFERENCES

- Arns, C. H., F. Bauget, A. Ghous, A. Sakellariou, T. J. Senden, A. P. Sheppard, R. M. Sok, W. V. Pinczewski, J. Kelly, and M. A. Knackstedt, "Digital core laboratory: Petrophysical analysis from 3D imaging of reservoir core fragments", *Petrophysics*, (2005), 46, 260-277
- Aste, T, "Volume fluctuations and geometrical constraints in granular packs", *Phys. Rev. Letters*. (2006), 96, 1
- Bakke S, P. Oren, "3-D pore scale modelling of heterogeneous sandstone reservoir rocks and flow simulations in the pore networks", *SPE* (1997) 35479
- Bryant S., M. Blunt, "Prediction of relative permeability in simple porous media", *Phys. Rev. A* 46 (1992), 2004-2011
- Bryant S., G. Mason, and D. Mellor, "Quantification of spatial correlation in porous media and its effect on mercury porosimetry", *J. Colloid Interface Sci.* (1996), 177, 88
- Bryant S.L., D. W. Mellor, C. A. Cade, "Physically representative network models of transport in porous media", *AIChE Journal* (1993), 39, 387
- Finney J., "Random packings and the structure of simple liquids I. the geometry of random close packing", *Proc R. Soc. London A* (1970), 319, 479
- Luchnikov V.A., N.N. Medvedev, L. Oger, J.P. Troadec, "Voronoi-Delaunay analysis of voids in systems of nonspherical particles", *Phys. Rev. E* (1999) 59, 7205-7212
- Richard P., L. Oger, J.P. Troadec, A. Gervois, "A model of binary assemblies of spheres", *Eur. Phys. J. E* (2001), 6, 295
- Thompson K.E., C. S. Willson, C. D. White, S. Nyman, J. Bhattacharya, A. H. Reid, "Application of a new grain-based reconstruction algorithm to microtomography images for quantitative characterization and flow modeling", *SPE* (2005) 95887
- Lindquist, W. B., S.-M. Lee, D.A. Coker, J.W. Jones, and P. Spanne, "Medial Axis Analysis of Void Structure in Three-Dimensional Tomographic Images of Porous Media", *J. Geophys. Res.* 101B, (1996) 8297-8310.
- Liang, Z., M. A. Ioannidis and I. Chatzis, "Geometric and topological analysis of three-dimensional porous media: pore space partitioning based on morphological skeletonisation", *J. Colloid Interface Sci.* (2000) 221, 13-24
- Silin, D, B. and T. W. Patzek, "Robust determination of the pore space morphology in sedimentary rocks", *Soc. Petrol. Eng. J.* (2003), 8429
- Al-Raoush, R. I. and C. S. Willson "Extraction of physically realistic pore network properties from three-dimensional synchrotron X-ray microtomography images of unconsolidated porous media systems", *J. Hydrology* (2005) 300, 44-64

15. Sakellariou, A., T. J. Sawkins, T. J. Senden and A. Limaye, "X-ray tomography for mesoscale physics applications", *Physica A*, (2004), 339, 152-158
16. Hilpert, M., and C. T. Miller, "Pore-morphology based simulation of drainage in totally wetting porous media", *Adv. Water Res.* (2001) **24**, 243-255
17. Pudney C., "Distance-Ordered Homotopic Thinning: A Skeletonization Algorithm for 3D Digital Images", *Comp. Vision Image Understanding*, (1998) 72, 404-413
18. Soille, P, "Morphological Image Analysis: Principles and Applications", Springer-Verlag, Berlin (2003)
19. Sheppard, A. P., R. M. Sok and H. Averdunk, "Techniques for image enhancement and segmentation of tomographic images of porous materials", *Physica A*, (2004) 339, 145-151
20. Sheppard A. P., R. M. Sok, H. Averdunk, "Improved methods for the extraction of pore networks", Society of Core Analysts Annual Meeting, Toronto, Canada (2005).

Sample	Voxel size ( $\mu\text{m}$ )	Subset Size (voxels)	Subset Size (mm)	Porosity (%)
U1	9.184	980 x 980 x 1860	9.0 x 9.0 x 18.0	23.2
U2	6.72	360 x 400 x 960	2.4 x 2.6 x 6.3	29
C1	3.024	900 x 900 x 1800	2.7 x 2.7 x 5.4	47
C2	2.604	1032 x 672 x 1128	2.7 x 1.74 x 2.9	12
S1	5.6	960 x 1056 x 1560	5.4 x 5.9 x 8.7	25.9
S2	4.928	928 x 1074 x 1600	4.5 x 5.3 x 7.9	21.6
S3	4.368	1120 x 1120 x 1960	5.0 x 5.0 x 8.6	

Table 1: Basic information on the 7 samples.

	$N_p$	$N_t$	$G_p (\text{mm}^{-3})$	$N_g$	$N_{gc}$	$G_g (\text{mm}^{-3})$	$D_g (\text{mm}^{-3})$
U1	201585	58791	103	32090	134436	74	NA
U2	42752	12836	713	6694	34028	651	60
S1	272422	102682	611	49809	308599	932	179
S2	206802	86533	248	34145	219731	383	179
S3	194289	93391	492	26520	185647	777	129
C1	149055	51333	2424	-	-	-	
C2	131245	67863	4589	-	-	-	

Table 2: Overall size and topological densities of the generated pore and grain networks.

	$\langle r_g \rangle$	$\langle \text{esr}_g \rangle$	$\langle S \rangle$	$\langle Z \rangle$	$\langle Z \rangle_v$	$\langle \text{AR} \rangle$	$\langle \text{AR} \rangle_v$	$\langle \text{RS} \rangle$
U1	10943	16366	0.67	8.6	21	4.5	9.0	4.56
U2	6513	9921	0.67	11	13	3.7	4.3	4.69
S1	6112	9324	0.66	13	18	3.4	4.0	4.57
S2	6112	9524	0.63	13	19	3.5	4.1	4.49
S3	7217	10732	0.67	14	22	3.6	4.3	4.26

Table 3: Results from the grain partitioning of clastic samples.

	$\langle r_p \rangle$	$\langle esr_p \rangle$	$\langle S \rangle$	$\langle Z \rangle$	$\langle Z \rangle_v$	$\langle AR \rangle$	$\langle AR \rangle_v$	$\langle RS \rangle$
U1	5420	10142	1.8	7.0	11	2.9	3.6	4.85
U2	248.8	5119	2.1	6.9	11	3.4	4.4	4.83
S1	238	4717	2.0	5.4	9.0	3.0	4.1	5.37
S2	198	4116	2.2	4.9	8.4	3.2	4.6	5.51
S3	198	3516	1.8	4.2	7.0	3.0	4.6	5.80
C1	1412	2720	1.9	5.6	30	6.5	20	-
C2	6.43.5	156.7	2.3	3.8	35	3.5	28	4.99

Table 4: Results from the pore partitioning

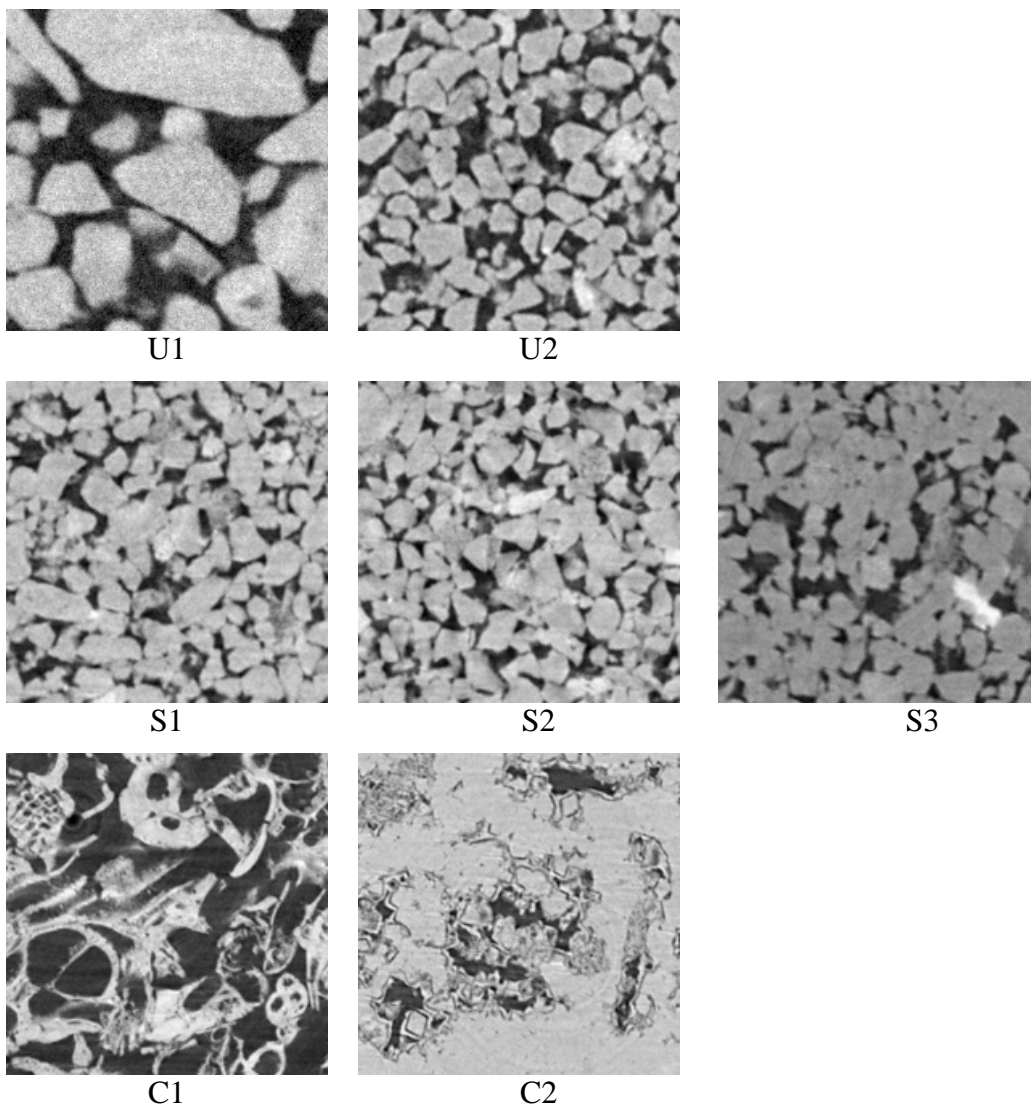


Figure 1: 1.8x1.8mm slices of raw reconstructed image data for the 7 core samples.

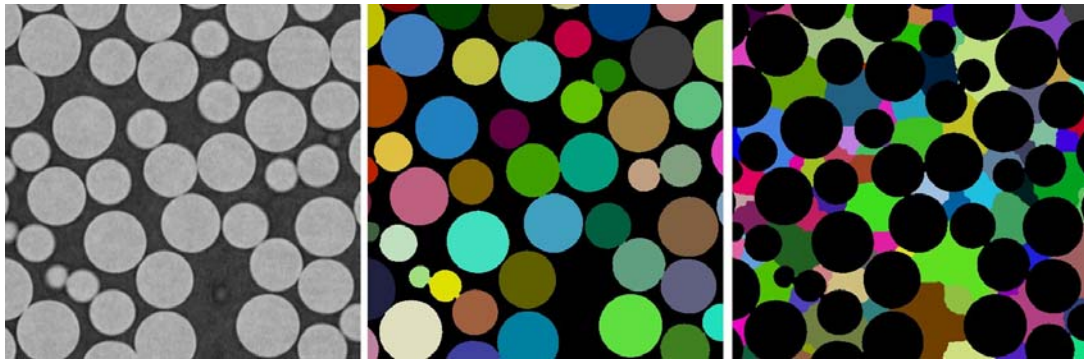


Figure 2: Images of monodispersed sphere pack P1. Left: raw reconstructed image data; Center: results of grain labeling; Right: results of pore labeling.

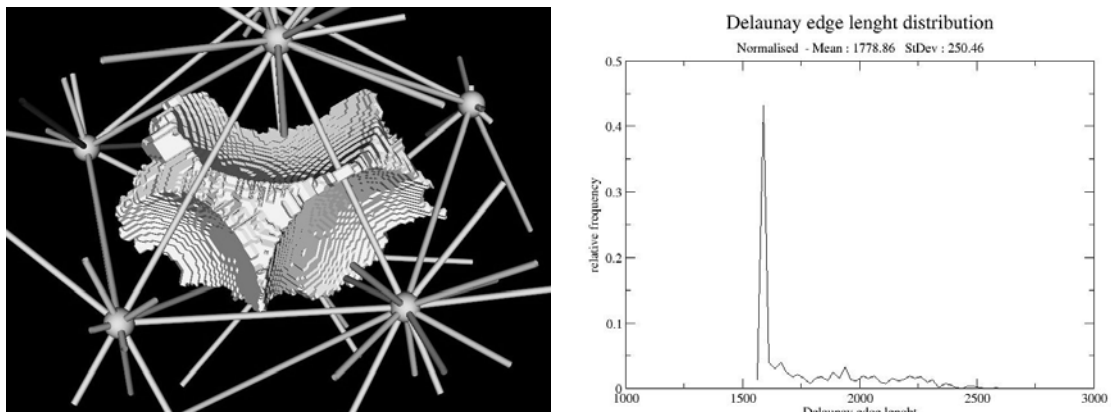


Figure 3: (a) Illustration of typical pore from sphere pack P1, overlaid with the Delaunay triangulation. The pore spans 3 Delaunay tetrahedra. (b) Distribution of Delaunay edge lengths (grain diameter is 1.56mm). Fewer than 50% of edges represent touching grains, while many connect widely separated grains.

Pore and Throat Radius Distributions

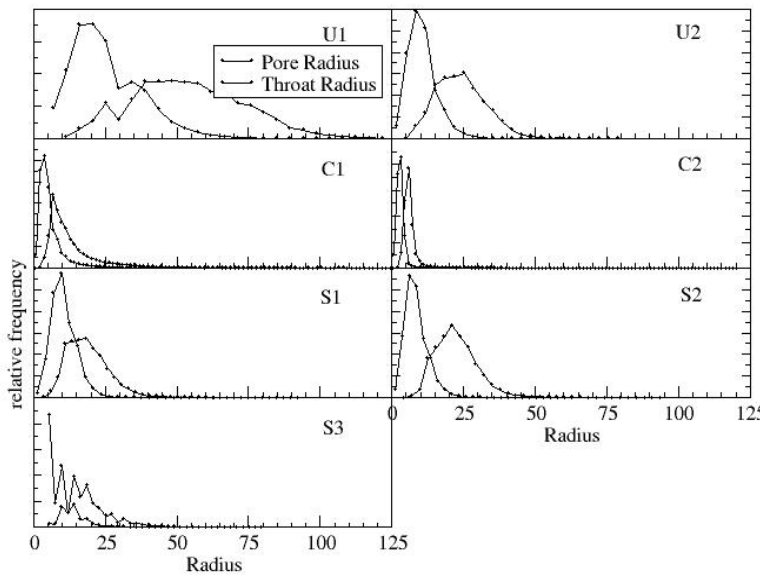


Figure 4: Pore and throat radius distributions of the 7 samples, weighted by number. Curves such as the throat distribution for S3 indicate a great deal of feature at or below the image voxel size. Note that without weighting this data by volume, the enormous but numerically insignificant pores in the carbonate samples are not visible.

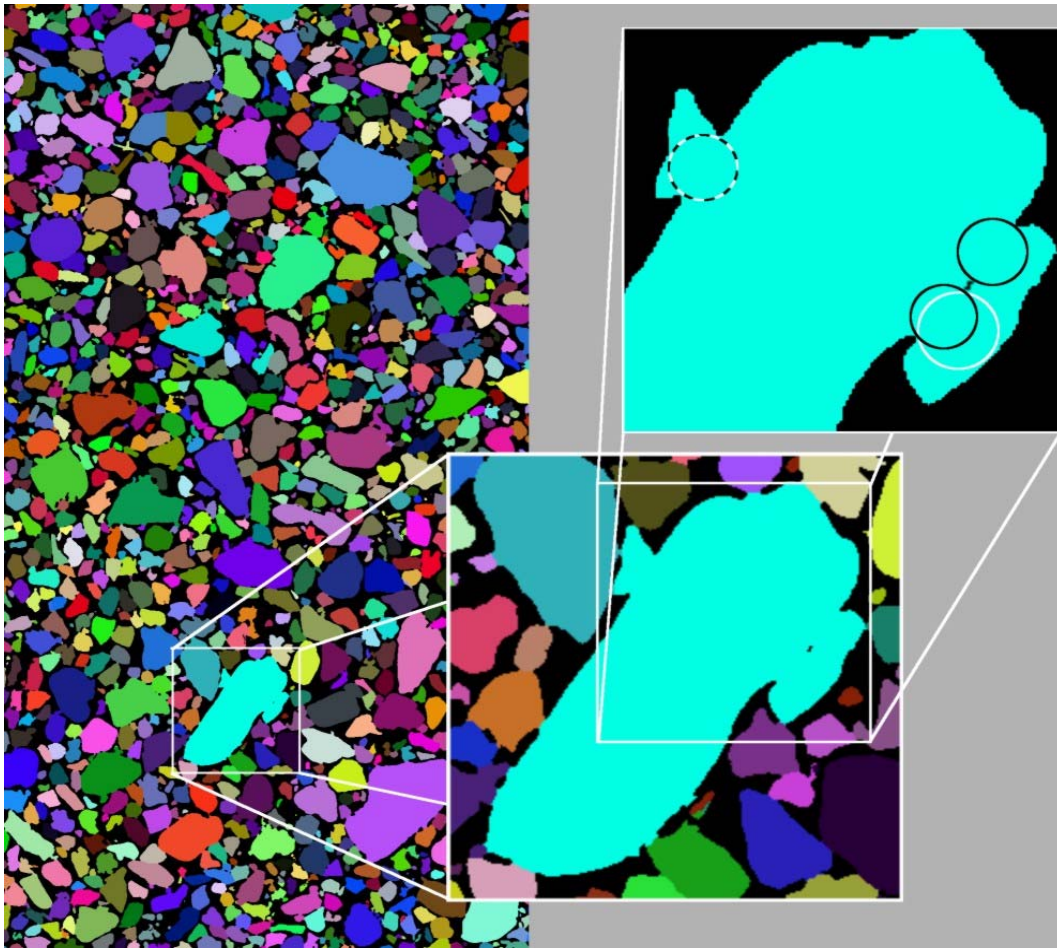


Figure 5: grain partitioning of the U1 unconsolidated fluvial sand. Inset shows detail of structure that is incorrectly labeled as a single grain, since the smaller grains attached are anisotropic. The schematic diagram shows the maximal inscribed Euclidean sphere in the bottom right attached grain as white circle and the maximal inscribed Euclidean sphere in the constriction as a black circle. It is clear that the maximal inscribed Euclidean spheres don't "see" the grain contact because they are constrained by the far side of the grain rather than by the intergranular constriction